

**Electron-impact excitation of krypton: Cross sections of interest in plasma modeling**R. K. Gangwar,<sup>1,2</sup> L. Sharma,<sup>3,4</sup> R. Srivastava,<sup>1</sup> and A. D. Stauffer<sup>2</sup><sup>1</sup>*Department of Physics, Indian Institute of Technology, Roorkee 247667 India*<sup>2</sup>*Department of Physics and Astronomy, York University, Toronto, Canada M3J 1P3*<sup>3</sup>*Physikalisches Institut, Universität Heidelberg, D-69120 Heidelberg, Germany*<sup>4</sup>*GSI Helmholtzzentrum für Schwerionenforschung GmbH, Planckstrasse 1, D-64291 Darmstadt, Germany*

(Received 23 June 2010; published 22 September 2010)

We have performed relativistic distorted-wave calculations to study the excitation of Kr from its ground  $4p^6$  configuration to the higher lying fine-structure levels of the  $4p^54d$ ,  $4p^55p$ , and  $4p^56s$  manifolds. We have obtained relativistic Dirac-Fock multiconfiguration wave functions for the ground and the excited states. We present results for differential cross section and compare these with the available experimental measurements for energies up to 100 eV. We also report integrated cross sections for incident electron energies up to 300 eV and provide analytic fits for plasma modeling applications.

DOI: [10.1103/PhysRevA.82.032710](https://doi.org/10.1103/PhysRevA.82.032710)

PACS number(s): 34.80.Dp

**I. INTRODUCTION**

Recently we have studied electron-impact excitation of argon gas atoms [1] in the light of the importance of optical emission diagnostics of rare-gas plasmas. These are widely used in laboratory and astrophysical plasma studies and industrial applications [2,3]. In [1] we used the relativistic distorted-wave (RDW) method to calculate differential cross sections (DCSs) for electron-impact excitation of argon atoms from the ground state to the various fine-structure levels of the  $3p^53d$ ,  $3p^55s$ , and  $3p^55p$  manifolds over a wide range of energies. We also reported angle-integrated cross sections (ICSs) for these transitions. Our RDW method is fully relativistic and utilizes the solution of the Dirac equations to calculate the wave functions of both the initial and final channels for the projectile electron. The bound target states are represented as Dirac-Fock multiconfiguration wave functions [1,4].

There has been a great deal of previous work on the excitation of krypton, but the vast majority has involved the  $4p^55s$  state. There has been little study of transitions to the higher lying fine-structure levels. Cross sections for these transitions are also needed for plasma modeling over a wide range of electron energies. In the present work we have applied our RDW method to calculate the excitation of the  $4p^54d$ ,  $4p^55p$ , and  $4p^56s$  manifolds of Kr from the ground state of the atom and report results for both DCS and ICS for incident-electron energies up to 300 eV. We also provide analytic fits to the ICS which are valid for higher energies and can be utilized for the plasma modeling. Although plasma modeling studies also require cross sections at lower energies, our present method is not reliable below about 20 eV incident energy. Thus other sources of cross sections, either experimental or theoretical, must be used to obtain a set of cross sections over the complete energy range starting from threshold. The DCS for various resolved and unresolved transitions are presented at 30, 50, and 100 eV where experimental results [5] exist. Until now there have been no theoretical results available except for excitation of the  $4p^55s$  and  $4p^55p$  levels.

Trajmar *et al.* [5] have reported DCS and ICS measurements for  $4p^55s$ ,  $4p^55p$ ,  $4p^54d$ , and  $4p^56s$  excitations from the ground state in the energy range 15–100 eV. They reported results for the  $4p^55s$  levels which were well resolved, but they were not able to resolve all of the levels of the  $4p^55p$ ,  $4p^54d$ , and  $4p^56s$

manifolds. For these states, results were published for a combination of various transitions. Their DCS measurements were in the range of  $10^\circ$ – $135^\circ$  scattering angles, and they extrapolated their measurements to forward and backward scattering angles to obtain ICS results. Later Chilton *et al.* [6] reported measurements for electron-impact excitation cross sections to various levels of the  $4p^55p$  manifold over a range of incident electron energies between threshold and 250 eV. Since they used an optical method, they obtained the direct excitation cross section by subtracting cascade contributions from their measured cross sections. Tsurubuchi *et al.* [7] also measured the apparent cross section for excitation of the  $4p^55s$  and  $4p^55p$  states, but since these cross sections include cascade contributions from higher states, they are not directly comparable to our calculations. Nevertheless, this paper did include comparison with earlier theoretical results for the direct cross sections [8,9].

Kaur *et al.* [8] used the RDW method to calculate the DCS and ICS for excitation of the  $4p^55p$  levels in the energy range 20–100 eV and where possible compared their results with the measurements of Trajmar *et al.* [5]. Dasgupta *et al.* [9] reported nonrelativistic and semirelativistic distorted-wave and close-coupling results for the ICS for excitation of the  $4p^55s$  and  $4p^55p$  levels of krypton in the range of incident electron energy from threshold to 50 eV. These included two types of distorted-wave results designated as DW-1 and DW-2 as well as 15- and 51-state Breit-Pauli *R*-matrix (BPRM) results. They compared their results with the theoretical results of Kaur *et al.* [8] and experimental measurements of Chilton *et al.* [6] and for some transitions with those of Trajmar *et al.* [5]. Guo *et al.* [10] reported DCS measurements for excitation of the  $4p^55p$ ,  $4p^54d$ , and  $4p^56s$  levels only at low electron-impact energies of 15 and 20 eV. They also included nonrelativistic *R*-matrix and unitarized first-order many-body theory (UFOMBT) calculations. Similarly, Zeng *et al.* [11] presented relativistic *R*-matrix calculations for energies below 20 eV for the excitation of the  $4p^55p$  levels from the ground state.

**II. THEORY****A. Wave functions**

The ground state of krypton has the configuration  $1s^22s^22p^63s^23p^63d^54s^24p^6$  in the *j-j*

TABLE I. Dipole oscillator strength for transition in Kr: measured values from Yuan *et al.* [13] and present calculations from GRASP2 K.

State	Ref. [13]	GRASP
$2s_4(J = 1)$	$0.147 \pm 0.010$	0.027
$2s_2(J = 1)$	$0.0079 \pm 0.0008$	0.024
$3d_1(J = 1)$	$0.045 \pm 0.003$	0.013
$3d_5(J = 1)$	$0.093 \pm 0.007$	0.281
$3d_{11}(J = 1)$	$0.0052 \pm 0.0003$	0.0053

coupling notation, where  $\bar{p}$ ,  $p$ ,  $\bar{d}$ ,  $d$  represent electron orbitals having total angular momentum  $j$  (orbital plus spin) of  $1/2$ ,  $3/2$ ,  $3/2$ , and  $5/2$ . The orbital angular momentum of these electrons is represented by the usual alphabetical notation. This state has even parity and total angular momentum  $J = 0$ . The  $4p^5 4d$  and  $4p^5 6s$  manifolds have odd parity and consist of 12 and 4 fine-structure levels, respectively. These are designated in Paschen notation as  $3d_k$ ,  $k = 1, 12$  and  $2s_k$ ,  $k = 2, 5$  in order of decreasing energy. We have carried out a multiconfiguration calculation for the wave functions of these levels as well as the ground state using the GRASP2 K program of Jönsson *et al.* [12]. We included configurations where one of the valence  $p$  orbitals is excited to the  $5s$ ,  $5\bar{p}$ ,  $5p$ ,  $4\bar{d}$ ,  $4d$ ,  $6s$ ,  $5\bar{d}$ ,  $5d$ ,  $6\bar{p}$ ,  $6p$ ,  $6\bar{d}$ , or  $6d$  orbitals. This gave 45 configurations with odd parity and 21 with even parity, but even with this large number of configurations, the oscillator strengths for the levels of interest for this work had not fully converged.

Only excited levels with odd parity and  $J = 1$  are connected to the ground state by an allowed transition and hence give rise to a dipole oscillator strength. We have compared our calculated values with those reported by Yuan *et al.* [13] in Table I. Our results for the  $3d_{11}$  level (which has the lowest energy of the levels shown) agree with the experimental measurements but are much less accurate for the other levels. As the energy increases, it becomes more difficult to obtain accurate oscillator strengths since the number of configurations which make a significant contribution increases. This lack of

convergence will affect the magnitude of our cross sections though not the energy dependence. The major contributions for each of these levels are given in Table II. Our calculations give an inverted order to the  $3d_9$  and  $3d_{10}$  levels which have almost identical energies. We have carried out similar calculations for the  $4p^5 5p$  manifold, which has even parity and 10 fine-structure levels designated in Paschen notation as  $2p_k$ ,  $k = 1, 10$ . For these levels, the configurations include the excited  $5\bar{p}$ ,  $5p$ ,  $6\bar{p}$ , and  $6p$  orbitals, and the coefficients are given in Table III.

## B. Calculation of DCS and ICS

The DCS in the RDW approximation for the electron impact excitation of an atom from initial state  $a$  to the final state  $b$  with total angular momentum  $J_a$  and  $J_b$ , respectively, is given by

$$\frac{d\sigma}{d\Omega} = (2\pi)^4 \frac{k_b}{k_a} |T_{a \rightarrow b}^{\text{RDW}}|^2,$$

where  $k_{a(b)}$  is the momentum of the projectile electron in the initial (final) channel and  $T_{a \rightarrow b}^{\text{RDW}}$  is the transition matrix for the excitation process which can be calculated as explained in our earlier work [1]. The transition matrix contains terms representing both direct excitation and transitions involving exchange of the incident electron with one of the bound electrons. The ICS is obtained by integrating the DCS over all scattering angles.

The initial ground state  $a$  of the Kr atom is closed shell having  $J_a = 0$ ; therefore, as explained in [1], the direct term of the  $T$  matrix is nonzero only if  $J_b$  is odd for the odd-parity ( $4d$  and  $6s$ ) states, while  $J_b$  must be even for the even-parity ( $5p$ ) state. In all other cases, only the exchange terms of the  $T$  matrix contribute to the cross sections. These exchange terms are in general much smaller than the direct term, especially at higher incident energies.

## III. RESULTS

### A. Differential cross sections

The DCS for various combined transitions to levels of the  $4p^5 4d$ ,  $4p^5 5p$ , and  $4p^5 6s$  manifolds are presented in

TABLE II. Major contributions of various configurations in the multiconfiguration wave functions of the  $4p^5 4d$  and  $4p^5 6s$  levels of Kr.

State	Major contributions
$4d'[3/2]_1$ $3d_1(J = 1)$	45.9% of $4\bar{p}^1 4p^4 4\bar{d}^1$ + 41.9% of $4\bar{p}^2 4p^3 5\bar{d}^1$ + 11.1% of $4\bar{p}^2 4p^3 5d^1$
$4d'[5/2]_3$ $3d_2(J = 3)$	67.4% of $4\bar{p}^1 4p^4 4d^1$ + 27.3% of $4\bar{p}^2 4p^3 5\bar{d}^1$ + 3.7% of $4\bar{p}^2 4p^3 5d^1$ + 1.0% of $4\bar{p}^2 4p^3 6\bar{d}^1$
$4d'[3/2]_2$ $3d_3(J = 2)$	82.1% of $4\bar{p}^1 4p^4 4\bar{d}^1$ + 11.3% of $4\bar{p}^1 4p^4 6s^1$ + 3.7% of $4\bar{p}^2 4p^3 5d^1$ + 1.7% of $4\bar{p}^1 4p^4 4d^1$
$4d'[5/2]_2$ $3d_4(J = 2)$	57.8% of $4\bar{p}^1 4p^4 4d^1$ + 30.8% of $4\bar{p}^2 4p^3 5d^1$ + 7.3% of $4\bar{p}^2 4p^3 5\bar{d}^1$ + 1.2% of $4\bar{p}^2 4p^3 4d^1$ + 1.0% of $4\bar{p}^1 4p^4 4\bar{d}^1$
$4d[3/2]_1$ $3d_5(J = 1)$	65.5% of $4\bar{p}^2 4p^3 4d^1$ + 26.5% of $4\bar{p}^2 4p^3 4\bar{d}^1$ + 3.2% of $4\bar{p}^2 4p^3 5d^1$ + 2.0% of $4\bar{p}^2 4p^3 6s^1$ + 1.0% of $4\bar{p}^1 4p^4 4\bar{d}^1$
$4d[5/2]_2$ $3d_6(J = 3)$	98.7% of $4\bar{p}^2 4p^3 4d^1$
$4d[5/2]_2$ $3d_7(J = 2)$	82.4% of $4\bar{p}^2 4p^3 4\bar{d}^1$ + 16.5% of $4\bar{p}^2 4p^3 4d^1$
$4d[7/2]_3$ $3d_8(J = 3)$	98.9% of $4\bar{p}^2 4p^3 4\bar{d}^1$
$4d[3/2]_2$ $3d_9(J = 2)$	72.1% of $4\bar{p}^2 4p^3 4d^1$ + 13.9% of $4\bar{p}^2 4p^3 4\bar{d}^1$ + 11.0% of $4\bar{p}^2 4p^3 6s^1$ + 2.0% of $4\bar{p}^1 4p^4 4d^1$
$4d[7/2]_4$ $3d_{10}(J = 4)$	99.8% of $4\bar{p}^2 4p^3 4d^1$
$4d[1/2]_1$ $3d_{11}(J = 1)$	66.8% of $4\bar{p}^2 4p^3 4\bar{d}^1$ + 27.4% of $4\bar{p}^2 4p^3 4d^1$ + 1.9% of $4\bar{p}^2 4p^3 6s^1$ + 1.2% of $4\bar{p}^1 4p^4 5s^1$ + 1.1% of $4\bar{p}^1 4p^4 4\bar{d}^1$
$4d[1/2]_0$ $3d_{12}(J = 0)$	95.9% of $4\bar{p}^2 4p^3 4\bar{d}^1$ + 1.8% of $4\bar{p}^1 4p^4 5s^1$ + 1.0% of $4\bar{p}^2 4p^3 6\bar{d}^1$ + 1.0% of $4\bar{p}^2 4p^3 5\bar{d}^1$
$6s[3/2]_2$ $2s_5(J = 2)$	88.4% of $4\bar{p}^2 4p^3 6s^1$ + 9.1% of $4\bar{p}^2 4p^3 4d^1$ + 2.3% of $4\bar{p}^2 4p^3 4\bar{d}^1$
$6s[3/2]_1$ $2s_4(J = 1)$	95.6% of $4\bar{p}^2 4p^3 6s^1$ + 3.9% of $4\bar{p}^2 4p^3 4\bar{d}^1$
$6s'[1/2]_0$ $2s_3(J = 0)$	85.6% of $4\bar{p}^1 4p^4 6s^1$ + 14.3% of $4\bar{p}^2 4p^3 5\bar{d}^1$
$6s'[1/2]_1$ $2s_2(J = 1)$	91.6% of $4\bar{p}^1 4p^4 6s^1$ + 5.1% of $4\bar{p}^2 4p^3 5\bar{d}^1$ + 2.1% of $4\bar{p}^2 4p^3 5d^1$ + 1.0% of $4\bar{p}^1 4p^4 4\bar{d}^1$

TABLE III. Coefficients of the various configurations in the multiconfiguration wave functions of the  $4p^55p$  levels of Kr.

Configuration	$4\bar{p}^24p^4$	$4\bar{p}^24p^35\bar{p}^1$	$4\bar{p}^14p^45\bar{p}^1$	$4\bar{p}^24p^35p^1$	$4\bar{p}^14p^45p^1$	$4\bar{p}^24p^36\bar{p}^1$	$4\bar{p}^14p^46\bar{p}^1$	$4\bar{p}^24p^36p^1$	$4\bar{p}^14p^46p^1$
$J = 0$ levels									
$1p_0$	1.0	–	0.0	0.0	–	–	0.0	0.0	–
$4p_5$	0.	–	–0.3056	0.9338	–	–	–0.0496	0.1796	–
$4p_1$	0.	–	0.8876	0.2085	–	–	–0.1160	0.3940	–
$J = 1$ levels									
$4p_{10}$	–	–0.6740	0.0692	0.7039	0.1974	–0.0452	–0.0135	0.0518	0.0396
$4p_7$	–	0.7201	–0.0951	0.6864	–0.0229	–0.0178	–0.0146	–0.0119	–0.0037
$4p_4$	–	0.0507	0.9714	0.0873	0.2079	–0.0258	0.0154	–0.0443	0.0046
$4p_3$	–	0.1504	0.1951	0.1540	0.9480	–0.0921	–0.0007	0.0917	0.0091
$J = 2$ levels									
$4p_8$	–	0.9975	–	0.1990	0.0683	0.0053	–	0.0005	–
$4p_6$	–	–0.1956	–	0.9789	–0.0278	0.0044	–	–0.0519	–
$4p_2$	–	–0.0773	–	0.0367	–0.0154	0.0528	–	0.9948	–
$J = 3$ levels									
$4p_9$	–	–	–	0.9997	–	–	–	0.0247	–

Figs. 1(a)–1(d) at incident electron energies of 30, 50, and 100 eV where the experimental results of Trajmar *et al.* [5] are available. The RDW calculations of the DCSs for individual and combined levels of the  $4p^55p$  manifold only have previously been reported in Kaur *et al.* [8] and compared with the data of Trajmar *et al.* [5] there. Although the results obtained in the present paper for  $4p^55p$  manifolds are calculated using more accurate multiconfiguration wave functions for both the ground and excited states, the results agreed with the results of Kaur *et al.* [8] to within 10%. Therefore we do not include comparisons of DCSs for transitions solely to the  $4p^55p$  manifolds in this paper.

In Fig. 1(a) we present the DCSs for the excitation to the combined levels  $3d_{11}$  and  $3d_{12}$  having  $J_b$  values 1 and 0,

respectively. The dipole allowed  $3d_{11}$  transition dominates in magnitude and shows a forward peak at all energies, while the purely exchange  $3d_{12}$  transition is almost flat in the forward direction. We observe that our summed theoretical results are in excellent agreement with the experimental measurements at all energies.

In Fig. 1(b), we show the DCSs for the excitation of the combined levels  $2p_2$ ,  $2p_3$ ,  $2p_4$ ,  $3d_8$ ,  $3d_9$ , and  $3d_{10}$  levels having  $J_b$  values 2, 1, 1, 3, 2, and 4, respectively. From these results we can observe the dependence of the DCS magnitude on  $J_b$ . The  $T$  matrices for the  $3d_8$  and  $2p_2$  transitions contain a direct term, while the remaining ones are purely exchange transitions and have smaller cross sections. Therefore both the former transitions dominate in magnitude and also show a forward

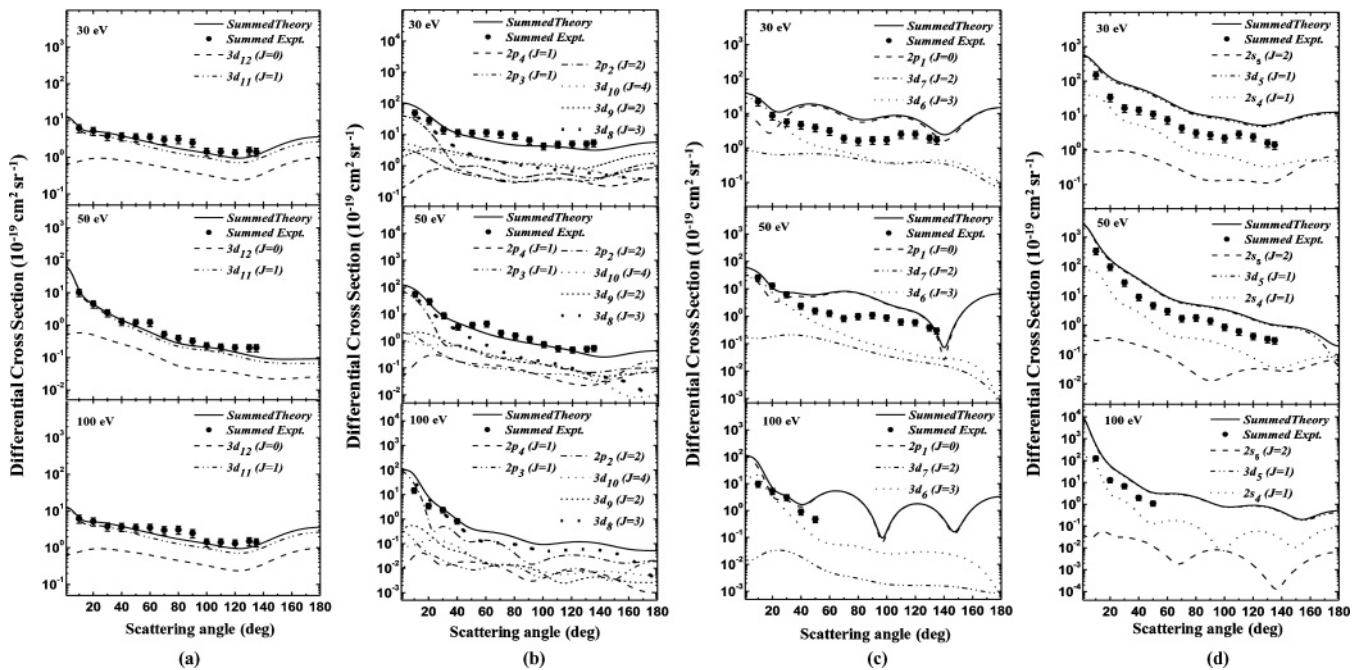


FIG. 1. Differential cross sections in units of  $10^{-19}$   $\text{cm}^2/\text{sr}$  for excitation of (a) the resolved and unresolved levels  $3d_{12}$  and  $3d_{11}$ ; (b) the resolved and unresolved levels  $2p_2$ ,  $2p_3$ ,  $2p_4$ ,  $3d_8$ ,  $3d_9$ , and  $3d_{10}$ ; (c) the resolved and unresolved levels  $2p_1$ ,  $3d_6$ , and  $3d_7$ ; and (d) the resolved and unresolved levels  $2s_5$ ,  $2s_4$  and  $3d_5$ . The solid circles are experimental data of Trajmar *et al.* [5].

peak in the cross section curve. Our combined DCS results are in very good agreement with the experimental measurements at most scattering angles.

Figure 1(c) displays the DCSs for the combined levels  $2p_1$ ,  $3d_7$ , and  $3d_6$  having  $J_b$  values 0, 2, and 3, respectively. The  $2p_1$  and  $3d_6$  transitions show the typical forward peaks of a direct transition with corresponding larger cross sections as compared to the purely exchange  $3d_7$  transition. The cross section for the  $2p_1$  transition with  $J_b = 0$  dominates, and while our results show reasonable agreement with the measurements at smaller scattering angles, deviations occur as the scattering angle increases. The fact that this level has the same parity and  $J$  value as the ground state makes it more difficult to obtain accurate results when using multiconfiguration wave functions.

Finally, in Fig. 1(d), we show the results for dipole allowed transitions  $2s_4$  and  $3d_5$  and for the forbidden purely exchange transition  $2s_5$  having  $J_b$  values 1, 1, and 2, respectively. The cross section for the  $3d_5$  transition is dominant over the entire angular range and is by far the largest contribution to the summed results. As expected, both the  $3d_5$  and  $2s_4$  transitions show forward peaks, while  $2s_5$  is almost flat in the forward angular region. Our combined results are higher in magnitude than the experimental measurements, although they show the same behavior. This is not unexpected since our calculated oscillator strength for the  $3d_5$  transition is much higher than the measured value as shown in Table I.

### B. Integrated cross sections

We have calculated the integrated cross sections for the excitation of all of the fine-structure levels of the  $4p^54d$ ,  $4p^55p$ , and  $4p^56s$  manifolds for incident electron energies up to 300 eV. For comparison, the experimental ICS results for combined unresolved levels are available from Trajmar *et al.* [5] for the same energies at which DCS results were reported. As pointed out earlier, they obtained ICS results by integrating their DCSs. Since their DCS measurements were made only in the range of  $10^\circ$ – $135^\circ$  scattering angles, they extrapolated their measurements to forward and backward angles to cover the entire angular range. This is a potential source of error if the extrapolations are not accurate. Chilton *et al.* [6] have also reported experimental measurements for the  $4p^55p$  manifold. Theoretical results were given by Dasgupta *et al.* [9] and Kaur *et al.* [8] for the same set of transitions. The former paper contains a detailed comparison with previous experimental and theoretical results, and since our present calculations are similar to those in [8] we do not repeat these here. Dasgupta *et al.* [9] pointed out significant disagreements between their theoretical results and the measurements of Chilton *et al.* [6]. We also observed similar differences which persist up to 250 eV. This is mostly likely because they must correct their measured values for cascade from upper levels to obtain the direct cross sections.

In Fig. 2, we compare our calculated ICSs for the excitation of fine-structure levels of the  $4p^54d$ ,  $4p^55p$  and  $4p^56s$  manifolds with the available experimental ICS results from Trajmar *et al.* [5] for incident electron energies up to 100 eV. We have also shown our theoretical results for the individual transitions which make up the combinations measured in [5]. Figure 2(a) contains the ICS for excitation of

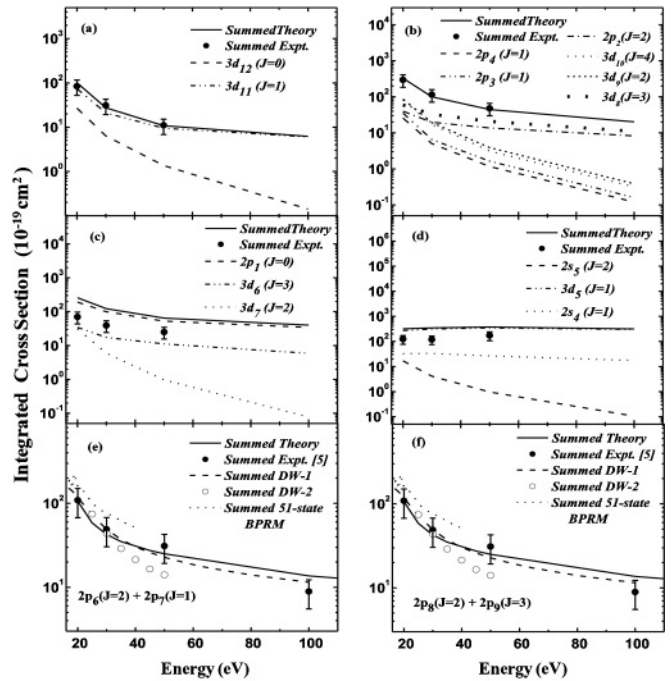


FIG. 2. Integrated cross sections in units of  $10^{-19}$  cm<sup>2</sup> for excitation of (a) the resolved and unresolved levels  $3d_{12}$  and  $3d_{11}$ ; (b) the resolved and unresolved levels  $2p_2$ ,  $2p_3$ ,  $2p_4$ ,  $3d_8$ ,  $3d_9$ , and  $3d_{10}$ ; (c) the resolved and unresolved levels  $2p_1$ ,  $3d_6$  and  $3d_7$ ; (d) the resolved and unresolved levels  $2s_5$ ,  $2s_4$ , and  $3d_5$ ; (e) the unresolved levels  $2p_6$  and  $2p_7$ ; and (f) the unresolved levels  $2p_8$  and  $2p_9$ . In Figs. 2(e) and 2(f), the different results are represented by solid lines, RDW calculations; dashed lines, DW-1 results [9]; open circles, DW-2 results [9]; and dotted lines, 51-state BPRM calculations [9]. The solid circles are experimental data of Trajmar *et al.* [5].

the  $3d_{12}$  ( $J_b = 0$ ) and  $3d_{11}$  ( $J_b = 1$ ) levels. Since the excitation of the  $3d_{12}$  level is a pure exchange transition, its cross section is much smaller than that for the  $3d_{11}$  transition. The agreement of our summed ICS with the experimental data is excellent.

In Fig. 2(b), we show the combined results for six levels:  $2p_2$  ( $J_b = 2$ ),  $2p_3$  ( $J_b = 1$ ),  $2p_4$  ( $J_b = 1$ ),  $3d_8$  ( $J_b = 3$ ),  $3d_9$  ( $J_b = 2$ ), and  $3d_{10}$  ( $J_b = 4$ ). Again, the agreement of our summed calculation with the experimental measurements is excellent. Here the transitions to the  $2p_2$  ( $J_b = 2$ ) and  $3d_8$  ( $J_b = 3$ ) levels are optically forbidden, but since they have a nonzero direct  $T$  matrix, they dominate at higher energies. Excitation of the other levels involves purely exchange transitions and these have significantly smaller cross sections.

Figure 2(c) displays the cross sections for three transitions:  $2p_1$  ( $J_b = 0$ ),  $3d_6$  ( $J_b = 3$ ), and  $3d_7$  ( $J_b = 2$ ). The  $2p_1$  transition has a nonzero direct  $T$  matrix and an unexpectedly large cross section. The excitation of the  $3d_6$  level also has a nonzero direct  $T$  matrix, but the cross section for this transition is much smaller. The transition to the  $3d_7$  level occurs only by exchange and has the smallest contribution. The agreement of our summed results with the experimental measurements is not very good because of the large cross section for the  $2p_1$  transition. This peculiar behavior of cross sections for excitation of even-parity levels with  $J_b = 0$  was also pointed out by Dasgupta *et al.* [9].

Figure 2(d) shows the results for three levels:  $2s_5$  ( $J_b = 2$ ),  $2s_4$  ( $J_b = 1$ ), and  $3d_5$  ( $J_b = 1$ ). The situation in this figure is similar to that in Fig. 2(c). Here the largest contribution comes from the cross section for the  $3d_5$  excitation followed by the  $2s_4$  excitation, and the least contribution comes from the purely exchange transition to the  $2s_5$  level. Our summed results are above the experimental data, as expected from the DCS results shown in Fig. 1(d).

In Figs. 2(e) and 2(f) we compare two sets of combined results from levels of the  $4p^55p$  manifold. In these figures we have also included the theoretical results DW-1, DW-2, and BPRM-51 from Dasgupta *et al.* [9]. Only the DW-1 results are available up to 100 eV (private communication). Figure 2(e) presents the results for excitation of the  $2p_6$  ( $J_b = 2$ ) and  $2p_7$  ( $J_b = 1$ ) levels. The largest contribution comes from excitation of the  $2p_6$  level since it has nonzero direct  $T$  matrix, while the  $2p_7$  transition is a pure exchange transition with correspondingly smaller cross section. We agree best with the theoretical DW-1 results over the energy range shown. The overall agreement of our summed results with the experimental data is excellent except at the largest energy where the measurement produces a smaller value than predicted by both theories. Figure 2(f) shows a similar comparison for excitation of the  $2p_8$  ( $J_b = 2$ ) and  $2p_9$  ( $J_b = 3$ ) levels. Here the larger contribution comes from the  $2p_8$  transition which has a nonzero direct  $T$  matrix, while the  $2p_9$  transition has a smaller cross section as expected from a purely exchange transition. Our RDW results are in good agreement with DW-1 calculations over this energy range. Our results also agree well with the measured values of Trajmar *et al.* [5] except at 100 eV where again the experimental result is lower than expected.

Finally in Figs. 3(a)–3(f) we show our ICS results in the range of 20–300 eV for all the transitions to the  $4p^55p$ ,  $4p^54d$ ,

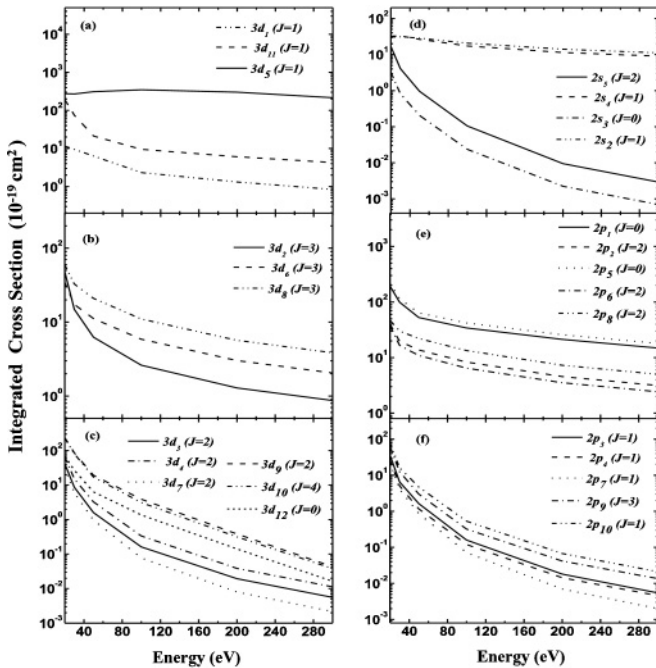


FIG. 3. Present integrated cross sections in units of  $10^{-19}$   $\text{cm}^2$  for excitation of the  $4p^55p$ ,  $4p^54d$ , and  $4p^56s$  manifolds.

TABLE IV. Fitting parameters  $b_0$  and  $b_1$  in Eq. (1) for the optically allowed transitions to the  $4p^54d$ , and  $4p^56s$  levels.

Racah Notation	Paschen notation	$b_0$	$b_1$
$4d'[3/2]_1$	$3d_1(J=1)$	0.027 61	0.002 69
$4d[3/2]_1$	$3d_5(J=1)$	0.755 62	2.473 00
$4d[1/2]_1$	$3d_{11}(J=1)$	0.033 47	0.040 22
$6s[3/2]_1$	$2s_4(J=1)$	0.106 28	0.100 47
$6s'[1/2]_1$	$2s_2(J=1)$	0.095 81	0.139 70

and  $4p^56s$  manifolds. The general behavior as a function of the parity and  $J_b$  value which we observed in Ar [1] are also present in the calculated ICS results of Kr. For example, the ICSs for pure exchange transitions drop off more rapidly with energy than those for which the direct  $T$  matrix is nonzero. For transitions for which the direct  $T$  matrix is nonzero, the value of  $J_b$  indicates the multipole moment of the interelectronic interaction which gives rise to this term. For the odd-parity levels, the transitions to the levels with total angular momentum  $J_b = 1$  are optically allowed dipole transitions and are expected to fall off more slowly with increasing impact energy than all the other transitions. The energy dependence of the cross sections as a function of  $J_b$  value is discussed further in the next section.

### C. Analytic fits to the integrated cross sections (in units of $a_0^2$ )

As an aid to the modeling of plasma processes, we have fitted our higher energy ICSs to an analytic formula. For the optically allowed transitions from the ground state to the excited  $4p^54d$  and  $4p^56s$  levels which have a value of  $J_b = 1$ ,

TABLE V. Fitting parameters  $c_0$  and  $c_1$  in Eq. (2) for the optically forbidden transitions to the  $4p^54d$ ,  $4p^55p$ , and  $4p^56s$  levels.

Racah notation	Paschen notation	$c_0$	$c_1$
$5p[1/2]_1$	$2p_{10}(J=1)$	0.101 27	-3.016 54
$5p[5/2]_3$	$2p_9(J=3)$	0.062 94	-3.012 72
$5p[5/2]_2$	$2p_8(J=2)$	0.134 68	-0.831 23
$5p[3/2]_1$	$2p_7(J=1)$	0.022 88	-3.393 52
$5p[3/2]_1$	$2p_6(J=2)$	0.066 67	-0.841 31
$5p[1/2]_0$	$2p_5(J=0)$	0.358 90	-0.698 83
$5p'[3/2]_1$	$2p_4(J=1)$	0.026 06	-3.098 30
$5p'[1/2]_1$	$2p_3(J=1)$	0.038 75	-3.188 26
$5p'[3/2]_2$	$2p_2(J=2)$	0.083 00	-0.823 29
$5p'[1/2]_0$	$2p_1(J=0)$	0.294 57	-0.698 06
$4d'[5/2]_3$	$3d_2(J=3)$	0.041 68	-1.097 27
$4d'[3/2]_2$	$3d_3(J=2)$	0.037 32	-3.151 10
$4d'[5/2]_2$	$3d_4(J=2)$	0.077 14	-3.161 03
$4d[5/2]_2$	$3d_6(J=3)$	0.071 08	-0.944 54
$4d[5/2]_2$	$3d_7(J=2)$	0.025 46	-3.396 38
$4d[7/2]_3$	$3d_8(J=3)$	0.133 68	-0.946 01
$4d[3/2]_2$	$3d_9(J=2)$	0.095 26	-3.216 34
$4d[7/2]_4$	$3d_{10}(J=4)$	0.073 21	-3.155 07
$4d[1/2]_0$	$3d_{12}(J=0)$	0.032 23	-3.157 94
$6s[3/2]_2$	$2s_5(J=2)$	0.025 25	-3.270 14
$6s'[1/2]_0$	$2s_3(J=0)$	0.005 21	-3.208 34

the ICSs are fitted by the formula

$$\text{ICS} = \frac{1}{E}[b_0 + b_1 \ln(E)]a_0^2. \quad (1)$$

Here,  $b_0$  and  $b_1$  are the fitting parameters and their values for the different allowed excitations are given in Table IV. The energy  $E$  is in atomic units (27.211 eV) and the ICS in units of  $a_0^2$  ( $0.280 \times 10^{-16}$  cm<sup>2</sup>). The fitted cross sections are valid for incident electron energies of 50 eV and above.

For the optically forbidden transitions, the ICS for the various excited levels of the  $4p^5 4d$  and  $4p^5 6s$  manifolds with  $J_b \neq 1$  as well as the parity forbidden transitions to the excited levels of the  $4p^5 5p$  manifold with all values of  $J_b$  are fitted by the expression

$$\text{ICS} = c_0 E^{c_1} a_0^2. \quad (2)$$

The units are the same as for (1). The fitting parameters  $c_0$  and  $c_1$  are given in Table V. The formula is valid for energy above 50 eV. As observed in our earlier work for Ar [1], for forbidden transitions which have a nonzero direct contribution to the  $T$  matrix ( $J_b$  odd and not equal to unity for the  $4p^5 4d$  and  $4p^5 6s$  manifolds or  $J_b$  even for the  $4p^5 5p$  manifold), the parameter  $c_1$  is approximately equal to  $-1$ , while for the purely exchange transitions ( $J_b$  even for the  $4p^5 4d$  and  $4p^5 6s$  manifolds or  $J_b$  odd for the  $4p^5 5p$  manifold), the parameter  $c_1$  is approximately equal to  $-3$ . The largest deviations from this pattern occur for the  $4p^5 5p$  levels with  $J_b = 0$ . As we noted earlier, these transitions cause some difficulty within a multiconfiguration approach to electron scattering (see also the discussion in [9]).

#### IV. CONCLUSIONS

We have used our RDW method to calculate cross sections for electron-impact excitation of the ground state of Kr to all fine-structure levels of the  $4p^5 4d$ ,  $4p^5 5p$ , and  $4p^5 6s$  manifolds. Our calculations generally agree well with the measured DCS and ICS of Trajmar *et al.* [5]. The major exception is the case of excitation of even-parity levels with  $J_b = 0$  which is the same as for the initial ground state. For these transitions, our calculated results appear to be too large. Otherwise, our results should be reliable for the energies reported here. We have observed the same behavior for the ICS as a function of parity and  $J_b$  value that we obtained in Ar [1].

To provide ICS results over a wide range of energies, we have fitted our cross sections to analytic formula. We expect that these data will be useful in plasma modeling studies.

#### ACKNOWLEDGMENTS

We are grateful to Dr. Arati Dasgupta for sending their theoretical results in the numerical forms. This research is supported in part by a grant to A.D.S. from NSERC Canada. R.S. acknowledges research grants in support of this work from the Council of Scientific and Industrial Research (CSIR), New Delhi, and IAEA, Vienna. R.K.G. is thankful to CSIR, New Delhi, and the Canadian Commonwealth Exchange Program (Asia-Pacific) for financial support. L.S. acknowledges support from the Helmholtz Gemeinschaft and GSI (Nachwuchsgruppe VH-NG-421).

- 
- [1] R. K. Gangwar, L. Sharma, R. Srivastava, and A. D. Stauffer, *Phys. Rev. A* **81**, 052707 (2010).
  - [2] J. B. Boffard, C. C. Lin, and C. A. DeJoseph, *J. Phys. D* **37**, R143 (2004).
  - [3] E. Gargioni and B. Grosswendt, *Rev. Mod. Phys.* **80**, 451 (2008).
  - [4] T. Zuo, R. P. McEachran, and A. D. Stauffer, *J. Phys. B* **24**, 2853 (1991).
  - [5] S. Trajmar, S. K. Srivastava, H. Tanaka, H. Nishimura, and D. C. Cartwright, *Phys. Rev. A* **23**, 2167 (1981).
  - [6] J. E. Chilton, M. D. Stewart Jr., and C. C. Lin, *Phys. Rev. A* **62**, 032714 (2000).
  - [7] S. Tsurubuchi, H. Kobayashi, and M. Hyodo, *J. Phys. B* **36**, 2629 (2003).
  - [8] S. Kaur, R. Srivastava, R. P. McEachran, and A. D. Stauffer, *J. Phys. B* **31**, 4833 (1998).
  - [9] A. Dasgupta, K. Bartschat, D. Vaid, A. N. Grum-Grzhimailo, D. H. Madison, M. Blaha, and J. L. Giuliani, *Phys. Rev. A* **64**, 052710 (2001).
  - [10] X. Guo *et al.*, *J. Phys. B* **33**, 1921 (2000).
  - [11] J. Zeng, J. Wu, F. Jin, G. Zhao, and J. Yuan, *Phys. Rev. A* **72**, 042707 (2005).
  - [12] P. Jönsson, X. He, C. Froese Fischer, and I. P. Grant, *Comput. Phys. Commun.* **177**, 597 (2007).
  - [13] Z. S. Yuan, L. F. Zhu, X. J. Liu, Z. P. Zhong, W. B. Li, H. D. Cheng, and K. Z. Xu, *Phys. Rev. A* **66**, 062701 (2002).